Journal of Materials Chemistry B

RSC Publishing

PAPER

View Article Online
View Journal | View Issue

Cite this: *J. Mater. Chem. B*, 2013, **1**, 284

Self-assembling doxorubicin prodrug forming nanoparticles for cancer chemotherapy: synthesis and anticancer study *in vitro* and *in vivo*

Pengfei Gou, Wenwen Liu, Weiwei Mao, Jianbin Tang, Youqing Shen and Meihua Sui*

The clinical utility of doxorubicin (DOX) is restricted by its severe side effects. Continuous efforts are aimed at developing efficacious DOX-delivery systems that may overcome the drawbacks of existing ones. Herein, we report a self-assembling prodrug forming high drug loading nanoparticles for DOX delivery. A low molecular weight polyethylene glycol (PEG) chain as the hydrophilic part was anchored to hydrophobic DOX *via* an acid-cleavable hydrazone bond to form the amphiphilic prodrug PEG–DOX. In aqueous solution, PEG–DOX formed nanoparticles with a diameter of ~125 nm and extremely high drug loading (~46 wt%). These nanoparticles were stable in PBS but released DOX in an acidic pH-triggered manner. Interestingly, taken up by cells *via* endocytosis, PEG–DOX bypassed the P-glycoprotein (P-gp)-mediated efflux of DOX, leading to drug accumulation in DOX-resistant human breast cancer cells (MCF-7/ADR). More importantly, PEG–DOX exhibited potent antitumor activity *in vitro* and *in vivo*, and showed significantly increased *in vivo* safety than free DOX. These encouraging data merit further preclinical and clinical development on PEG–DOX.

Received 22nd August 2012
Accepted 16th October 2012

DOI: 10.1039/c2tb00004k

www.rsc.org/MaterialsB

1 Introduction

As a most widely used anticancer drug approved by FDA, doxorubicin (DOX) is crucial to the treatment of a range of neoplasms such as breast, ovarian, and gastric cancers and acute lymphoblastic-leukemia, alone or in combination with other agents.[1–5] Many studies have attributed the antitumor activity of DOX to its ability to intercalate into the DNA helix and/or bind covalently to proteins involved in DNA replication and transcription, as well as act as a topoisomerase II poison, all of which ultimately lead to cell death.[6–8] However, its severe toxic side effects, especially its cardiotoxicity, greatly limit its clinical use.[9–11] Several lines of investigation are ongoing to improve the outcome of DOX treatment, *e.g.* seeking DOX analogs, development of efficacious DOX-delivery systems.[5] An efficacious DOX-delivery system holds the promise to increase the drug concentration at its site of action and meanwhile to reduce its side effects in non-target tissues, and thus has become a major strategy to improve the outcome of DOX treatment.

During the past few years, significant progress has been made towards the design and synthesis of nanoscale DOX-delivery systems such as nanoparticles, polymeric micelles, dendrimers, liposomes and polymer conjugates.[12–20] Among them, liposomal formulations of DOX have been approved for clinical use,[17] while polymeric micelles loaded with DOX are currently being evaluated in clinical trials.[18–20] Such nanosized vehicles could greatly enhance the drugs' water solubility and stability, prolong their circulation in blood compartments, target cancerous tissues by passive accumulation *via* tumor's enhanced permeability and retention (EPR) effect and targeting groups such as folic acid (FA) and epidermal growth factor (EGF).[21–24] Therefore, drugs in the nanocarriers have shown therapeutic advantages including better antitumor activity and fewer side effects over free drugs. These drug carriers, however, are usually associated with some inherent drawbacks, especially low drug loading and premature burst release.[25–29] For example, many reported DOX-delivery systems have very low drug loading capacity (usually less than 10 wt%).[26,27] Moreover, repeated administration of large amounts of inactive carriers to patients may induce systemic toxicity and even severe allergic reactions.[28]

To develop more efficacious DOX-delivery systems, we herein designed and synthesized a novel DOX prodrug, PEG–DOX, by conjugating a deprotonated DOX molecule with a short chain of polyethylene glycol (PEG) molecule *via* a hydrazone bond, forming a prodrug in which DOX itself is the hydrophobic segment and PEG is regarded as the hydrophilic segment. This amphiphilic prodrug is expected to self-assemble into stable nanoparticles in aqueous solutions and thus may take advantage of the EPR effect. As a result of the

Key Laboratory of Biomass Chemical Engineering of Ministry of Education, Center for Bionanoengineering and State Key Laboratory of Chemical Engineering, Department of Chemical and Biological Engineering, Zhejiang University, Hangzhou, China, 310027. E-mail: suim@zju.edu.cn; Fax: +86 571 87951493; Tel: +86 571 87951493

low molecular weight of PEG and the well-defined structure of PEG–DOX, the nanoparticles have a high and fixed DOX loading content. Moreover, PEG is a well-known and widely used polymer carrier for drug delivery since it has been approved for clinical use.[30–33] Particularly, modification with PEG (PEGylation) has been shown to significantly improve the physicochemical and biological properties of various drug delivery systems.[34–36] Furthermore, DOX is conjugated with PEG *via* a hydrazone bond, a well-known pH-responsive bond,[37,38] which may induce faster release of DOX in an acidic environment (*e.g.* endo-lysosomes) than under neutral conditions (*e.g.* blood circulation). This novel prodrug was carefully characterized and its biological effects were evaluated using a series of *in vitro* and *in vivo* assays. The obtained data demonstrated that PEG–DOX has multiple advantages and holds promise to become an alternative to the free drug DOX for cancer chemotherapy.

2 Experimental

2.1 Materials

Doxorubicin·HCl (DOX·HCl) was supplied by Zhejiang Hisun Pharmaceutical Co. (Taizhou, China). Methoxypolyethylene glycol (PEG-OH, M_w 550 Da) and trifluoroacetic acid (TFA) were obtained from Aladdin Chemistry Co. (Shanghai, China). Ether absolute was obtained from Hangzhou Chemical Reagent Co. (Hangzhou, China). Sodium hydride (NaH) was purchased from Sigma-Aldrich (Shanghai, China). All other chemicals were purchased from Sinopharm Chemical Reagent Co (Shanghai, China). Buffers used in this study were all filtered through a 0.22 μm filtering membrane prior to use. A549 (human lung cancer), SKOV3 (human ovarian cancer), BCap37 and MCF-7/ADR (both human breast cancer) cell lines were obtained from the American Type Culture Collection and/or have been used in our previous studies.[39,40] Six-to-eight-week old female BALB/c homozygous athymic nude mice were purchased from the Animal Center of Zhejiang University, and maintained under standard conditions. The use of animals for *in vivo* studies was approved by the Animal Ethics Committee in Zhejiang University.

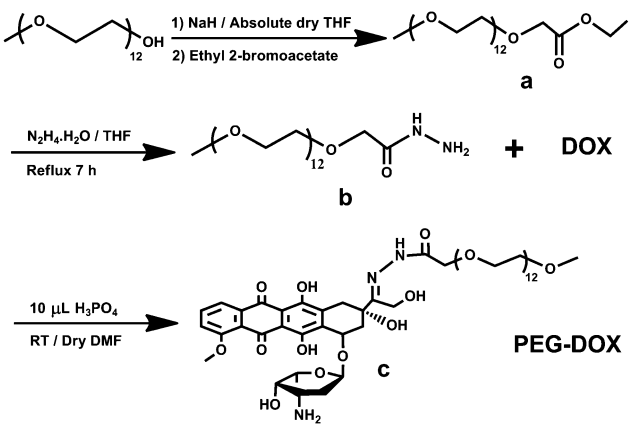

Fig. 1 Synthesis of PEG–DOX.

2.2 Preparation of PEG–DOX prodrug

The reaction scheme for the synthesis of PEG–DOX is depicted in Fig. 1, and could be described as a three-step process.

2.2.1 Synthesis of ethyl α-PEGoxyacetate (PEG–O–CH_2COOEt, compound a). PEG–O–CH_2COOEt was prepared using a two-step reaction procedure. PEG–OH (5.5 g, 10 mmol) and 30 mL absolute tetrahydrofuran (THF) were added to a completely dry flask under dry Ar protection. NaH (0.72 g, 30 mmol) was quickly added to the mixture with stirring at room temperature. The mixture was allowed to react for 6 h until no bubbles emerged. Ethyl bromoacetate (2 g, 12 mmol) was then injected into the mixture. Two hours later, 5 mL water was carefully added to terminate the reaction. The THF was removed under vacuum and the resulting mixture was extracted with dichloromethane (CH_2Cl_2, 20 mL × 3). The organic phase was collected and the solvent was removed under vacuum. The crude product was further purified with *n*-hexane precipitation three times and then PEG–O–CH_2COOEt (3.1 g, yield 49%) was obtained and confirmed by ^1H NMR.

2.2.2 Synthesis of α-PEGoxyacetylhydrazine (PEG–O–$CH_2CONHNH_2$, compound b). PEG–O–CH_2COOEt (1.9 g, 3 mmol) and hydrazine hydrate (15 g, 300 mmol) were mixed with 100 mL THF in the flask, and the mixture was refluxed with vigorous stirring for 7 h. The THF (upper) phase was obtained and the solvent was removed under vacuum. The crude product was further purified with ether precipitation three times and PEG–O–$CH_2CONHNH_2$ (1.5 g, yield 80%) was obtained and confirmed by ^1H NMR.

2.2.3 Synthesis of PEG–DOX (compound c). DOX·HCl (0.29 g, 0.5 mmol) and PEG–O–$CH_2CONHNH_2$ (0.93 g, 1.5 mmol) were dissolved in 15 mL of anhydrous dimethylformamide (DMF), and 10 μL phosphoric acid was added as a catalyst. The mixture was stirred in the dark at room temperature for 48 h. Then 100 μL triethylamine (TEA) was added and the mixture was dialyzed using a dialysis bag (molecular weight cut-off 3500 Da) against weak alkaline PBS (pH 8.0) for 48 h. After freeze-drying, the final product PEG–DOX (0.52 g, yield 90%) was obtained, and confirmed by ^1H NMR and high-performance liquid chromatography (HPLC).

2.3 Preparation and observation of nanoparticles from PEG–DOX

PEG–DOX nanoparticles were prepared using the nano-precipitation method. Typically, 1 mg PEG–DOX was dissolved in 500 μL THF, and the solution was added dropwise to a weak alkaline PBS with vigorous stirring within 5 min in the dark. Thereafter, the solvent THF was removed under vacuum slowly, and the PEG–DOX nanoparticles were obtained and characterized by Dynamic Light Scattering (DLS) and Transmission Electron Microscopy (TEM). For TEM observation, typically, one drop of the PEG–DOX nanoparticles was placed on a copper grid covered with a nitrocellulose membrane and drained by filter paper and then stained with uranyl acetate (UA) solution. The solution was drained with filter paper again and finally air-dried in the dark. Observations were carried out using a JEOL-JEM-1230 TEM (Tokyo, Japan).[39]

2.4 Determination of drug release

PEG–DOX nanoparticles at a concentration of 0.2 mg mL^{-1} were prepared as described above (Section 2.3) and incubated at 37 °C in PBS (pH 4.0, 5.0 and 7.4). At specific time intervals, samples (0.2 mL) were withdrawn and analyzed by HPLC using an XBridge™ C_{18} reverse phase column (4.6 × 250 mm, 5 μm) with UV detection at 480 nm at 35 °C. A gradient elution of 60–90% methanol–water both containing 0.05% TFA was applied at a flow rate of 1 mL min^{-1}. During assays, 20 μL of each sample was injected into the analytic column. The release of DOX was detected by UV at 480 nm, and the hydrolysis degree was determined based on the ratio of free DOX peak areas to the corresponding PEG–DOX peak areas.

2.5 3-(4,5-Dimethylthiazolyl-2)-2,5-diphenyltetrazolium bromide (MTT) assay

The *in vitro* antitumor activity of PEG–DOX nanoparticles and free DOX was assessed using MTT assays in A549, SKOV3 and BCap37 cell lines. Typically, adherent tumor cells (5000–6000 cells per well) were evenly plated into 96-well plates and incubated overnight. Then cells were exposed to serial dilutions of PEG–DOX or DOX and further incubated for 48 h. Thereafter the plates were centrifuged to collect all the cells, washed three times with PBS and incubated for another 24 h with fresh medium. Subsequently, the medium in each well was replaced with fresh medium containing 1 mg mL^{-1} MTT and incubated for an additional 3 h. Finally, dimethyl sulfoxide (DMSO) was used to dissolve the formazan crystals. The absorbance was determined at 562 nm with a microplate spectrophotometer (Molecular Devices, SpectraMax M2e, USA).

2.6 Cellular uptake observed by confocal laser scanning microscopy (CLSM)

The cellular uptake of PEG–DOX nanoparticles and DOX was examined in both SKOV3 (P-gp non-expressing) and MCF-7/ADR (P-gp overexpressing) cell lines. Briefly, tumor cells were plated onto glass-bottomed Petri dishes in 1.5 mL of complete culture medium for 24 h before treatment. Then cells were treated with free DOX solution (5 μg mL^{-1}) or PEG–DOX nanoparticles (equivalent to 5 μg mL^{-1} DOX) for designated time periods. For SKOV3 cells, LysoTracker (Molecular Probes, USA) was directly added to the medium at a final concentration of 300 nM for 2 h to label lysosomes. For MCF-7/ADR cells, DRAQ-5 (Cell Signaling Technology, USA) was added to the medium for 30 min to label the nucleus. The tumor cells were washed three times with fresh medium and the images were taken using a CLSM (Nikon-A1 system, Japan). The fluorescence characteristics of DOX and PEG–DOX were used to directly monitor localization of these drugs without utilizing additional dye ($\lambda_{ex} = 480$ nm, $\lambda_{em} = 600$ nm).

2.7 *In vivo* evaluation on antitumor efficacy and safety

To evaluate the *in vivo* antitumor activity of PEG–DOX nanoparticles and their potential toxicity to normal organs, we developed human xenograft tumor models through transplanting SKOV3 cells into the right flanks of nude mice (1×10^6 cells per mouse). When tumors reached a mean diameter of around 4 mm (usually 7–10 days after implantation), mice were randomly divided to three groups ($n = 4$ per group): CTL (PBS); DOX dissolved in PBS (10 mg kg^{-1}, a dose close to the maximum tolerated dose (MTD) as previously reported);[41] PEG–DOX solution (equivalent to 10 mg kg^{-1} DOX). The treatments were initiated on day 0 (i.v.) and repeated every 3 days. The antitumor efficacy of the designed treatments was assessed by tumor volume change and tumor growth inhibition rate,[42,43] while the treatment-induced systemic toxicity/adverse side effects were evaluated by body weight changes in animals. At the end of the experiments, all animals were sacrificed according to institutional guidelines. Xenograft tumor and the heart, a particularly susceptible organ to DOX-induced toxicity, of each animal were resected and fixed with 4% neutral buffered paraformaldehyde and embedded in paraffin. Tissue sections were prepared and stained with hematoxylin and eosin (H&E, Fisher Scientific, USA) for histological examinations. The histological identification of apoptotic tumor cells and toxicity of DOX to cardiomyocytes have been described in previous publications.[41,44,45]

2.8 Statistical analysis

Data are presented as mean ± standard error. Changes in tumor volume and body weight over time were analyzed by one-way ANOVA (analysis of variance) and subsequently by Student's *t*-test. All other statistical analyses were performed using Student's *t*-test. Differences were considered statistically significant at a level of $p < 0.05$.

3 Results and discussion

3.1 Synthesis and characterization of PEG–DOX

As described above, PEG–DOX was synthesized by using a three-step procedure. The obtained PEG-O-CH_2COOEt was confirmed by ^1H NMR (400 MHz, $CDCl_3$): δ (ppm) 4.26 (2H, m, CH_2), 4.13 (2H, s, CH_2), 3.63 (48H, m, $-OCH_2CH_2O-$), 3.36 (3H, s, CH_3), 1.26 (3H, t, CH_3) (Fig. 2A). The peaks at 3.5–3.7 and 3.36 ppm were attributed to the protons of the main chain of PEG and the terminal methyl group of PEG, respectively. The signals at 4.26 and 1.26 ppm were observed due to the methylene connecting the main chain of PEG and the terminal methyl of alcohol. In the second step, the successful synthesis of PEG-O-$CH_2CONHNH_2$ was confirmed by ^1H NMR (400 MHz, $CDCl_3$): δ (ppm) 4.04 (2H, s, CH_2), 3.68 (48H, m, $-OCH_2CH_2O-$), 3.34 (3H, s, CH_3) (Fig. 2B). The signals of the PEG main chain and terminated methyl group were also observed at 3.5–3.7 and 3.36 ppm. Finally, PEG–DOX was synthesized by the reaction of the hydrazide bond of PEG-O-$CH_2CONHNH_2$ with the carbonyl bond of DOX, and the obtained PEG–DOX was confirmed by ^1H NMR and HPLC. The successful conjugation of PEG with DOX was proven by the peaks at 3.5–3.7 and 3.36 ppm in the PEG–DOX ^1H NMR spectrum when compared to that of DOX (Fig. 2C and D). Meanwhile, the retention time of DOX was 6.37 min

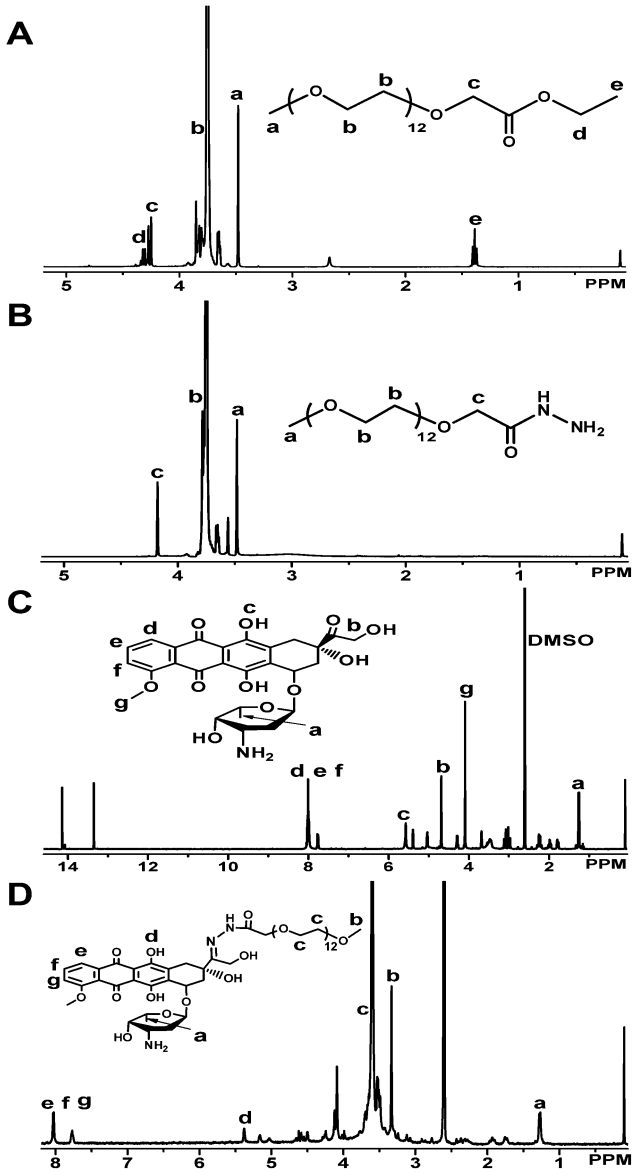

Fig. 2 ^{1}H NMR spectra of PEG-O-CH_2COOEt in $CDCl_3$ (A), PEG-O-CH_2CONHNH_2 in $CDCl_3$ (B), DOX·HCl in d-DMSO (C) and PEG–DOX in d-DMSO (D).

while that of PEG–DOX was 14.96 min under the given experimental conditions (Fig. 3A and B).

The obtained PEG–DOX could self-assemble to form stable nanoparticles in PBS (pH 7.4) because of its amphiphilic structure, with high uniformity and good transparency. These nanoparticles had a *z*-average particle size of ~125 nm and a polydispersity index (PDI) of 0.24 (Fig. 3C). The structure of the particles was further confirmed by TEM. UA is water-soluble and thus stains the hydrophilic region. The TEM image with a bright core indicates that the amphiphilic prodrug PEG–DOX indeed formed ~100 nm nanoparticles (Fig. 3C), which may enable PEG–DOX to passively target tumor tissues *via* the EPR effect.

PEG–DOX is very different from the reported water-soluble polymer–DOX prodrugs or conjugates, in which high-molecular-weight hydrophilic polymers are usually used to ensure their water-solubility, resulting in very low drug loading contents. For instance, *N*-(2-hydroxypropyl)-methacrylamide (HPMA)–doxorubicin conjugate (PK1; FCE28068) and HPMA copolymer–doxorubicin–galactosamine conjugate (PK2; FCE28069) currently tested in clinical trials have a drug loading content of only ~8 wt% for PK1 and even lower for PK2.[16,18] In contrast, we herein on purpose used a low molecular weight PEG to make amphiphilic PEG–DOX, which is not molecularly water-soluble but capable of self-assembling into nanoparticles having a fixed drug loading content as high as ~46 wt%, much higher than all the other reported DOX–polymer conjugates. Moreover, the PEG-corona is expected to effectively reduce the non-specific uptake by the reticuloendothelial system (RES), prolong circulation time and allow for specific tumor-targeting through the EPR effects.[46]

3.2 Drug release profile

The drug release profile of PEG–DOX nanoparticles was assessed under a simulated physiological condition (PBS, pH 7.4) and under acidic conditions (PBS, pH 5.0 and 4.0) simulating the endo-lysosomal environment at 37 °C. As reported previously,[31,32] the hydrazone linkage has a characteristic pH-responsive behavior, which may result in a favorable pH-dependent release profile of DOX from PEG–DOX nanoparticles. Indeed, as depicted in Fig. 3D, we observed that PEG–DOX was quite stable at pH 7.4, but exhibited a much faster release of DOX at pH 4.0 and 5.0. Thus, the hydrazone linkage enables PEG–DOX to remain stable in the blood circulation and thereby eliminates the premature burst release, while effectively promoting DOX release from its prodrug once cleaved in the target sites (*e.g.* acidic tumor extracellular environment, endo-lysosomes). In contrast to conventional liposomal DOX whose clinical applications were limited by its poor stability and subsequently undesirable drug burst release,[15] the pH-responsiveness of these nanoparticles, together with the above-mentioned passive target ability due to EPR effect, will assist PEG–DOX in achieving an effective concentration of DOX in tumor cells and meanwhile reducing the unexpected premature burst release.

3.3 *In vitro* antitumor activity

In MTT assays, we observed that SKOV3 cells were more sensitive to DOX and PEG–DOX than A549 and BCap37 cells (Fig. 4). Although PEG–DOX nanoparticles showed decreased toxicity compared to free DOX, they still exhibited significant *in vitro* antitumor activity. For instance, the half maximal inhibitory concentration (IC_{50}) values for PEG–DOX against SKOV3, A549 and BCap37 cell lines were 0.086 μg mL^{-1}, 0.123 μg mL^{-1} and 0.429 μg mL^{-1}, respectively, while those for free DOX were 0.0164 μg mL^{-1}, 0.0243 μg mL^{-1} and 0.156 μg mL^{-1}, respectively ($p < 0.05$, PEG–DOX *versus* DOX in all three cell lines). It is well-known that free DOX permeates cellular and nuclear membranes by passive diffusion.[47] However, PEG–DOX nanoparticles are expected to be taken up by tumor cells *via* endocytosis, followed by endo-lysosomal escape and subsequent drug distribution in the cytosol and nucleus. These processes are much slower than passive diffusion and would result in slow

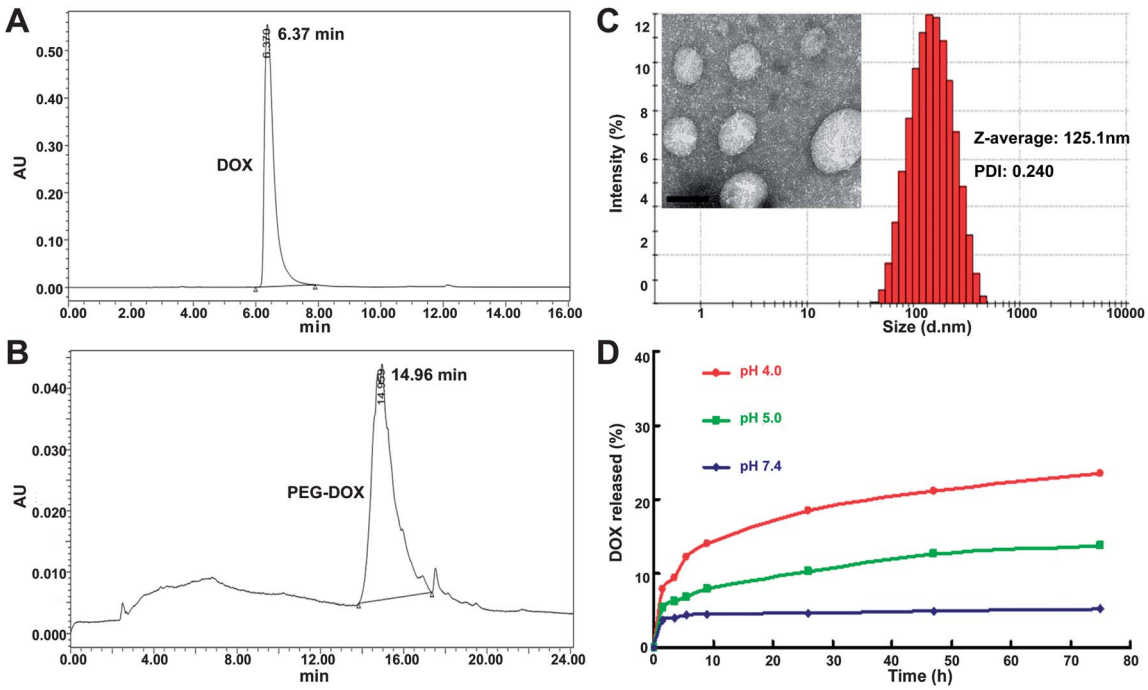

Fig. 3 HPLC traces of DOX (A) and PEG–DOX (B) under the given HPLC conditions; size and size distribution by intensity, and the TEM image of PEG–DOX nanoparticles stained with water-soluble uranyl acetate (C); DOX release profile from the PEG–DOX at pH 4.0, 5.0 and 7.4 (D), respectively. Scale bar = 100 nm in TEM image.

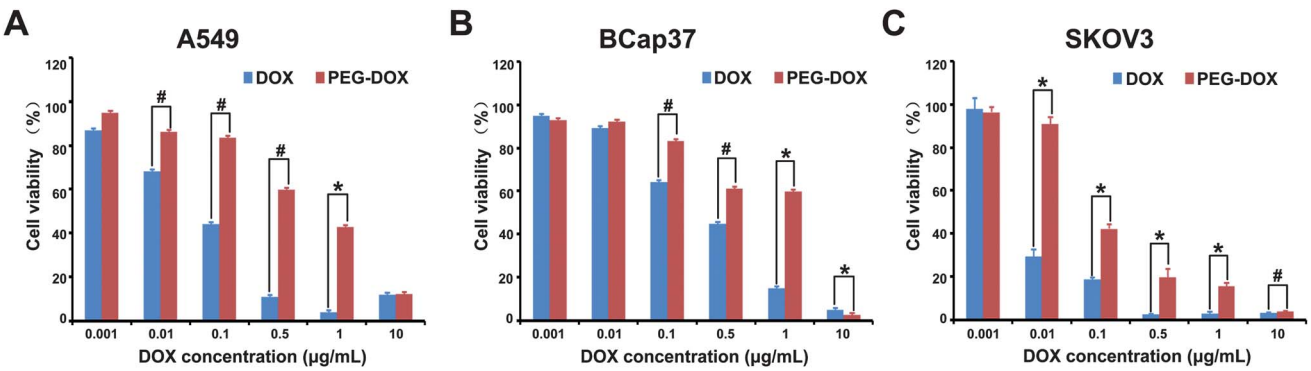

Fig. 4 The cytotoxicities of free DOX and PEG–DOX against A549, BCap37 and SKOV3 cells, respectively, as determined by MTT assay. Cells were treated with designated regimes for 48 h followed by 24 h incubation with fresh medium. Data represent mean ± standard deviations (SD), $n = 3$. $^{\#}$, $P < 0.05$; *, $P < 0.001$.

release of conjugated DOX from PEG–DOX. In fact, this is one common reason why drugs delivered in nanocarriers usually have lower *in vitro* activity than original small molecular drugs.

3.4 Cellular uptake and intracellular localization

As mentioned above, DOX and PEG–DOX have inherent fluorescence, they were thus directly observed with CLSM (shown in red), and the fluorescence intensity detected in cells treated with PEG–DOX or DOX coincides with the concentration of DOX internalized into the cells. Meanwhile, LysoTracker and DRAQ-5 were used to label the lysosomes (shown in green) and the nucleus (shown in blue), respectively. As shown in Fig. 5A–C, after incubation with free DOX for 5 h, the red and green fluorescence in SKOV3 cells did not co-localize with each other, which is consistent with the diffusion pathway by which free DOX enters cells.[47] In contrast, PEG–DOX nanoparticles mainly enter cells *via* endocytosis, as demonstrated by the co-localization of drug and lysosomes (Fig. 5D–F, yellow spots indicating overlay of red and green fluorescence). More importantly, in P-gp-overexpressing MCF-7/ADR cells, the fluorescence of DOX was almost invisible in the cytoplasm and nucleus after cells were incubated with free DOX for 5 h. Instead, DOX was only observed on the cell membrane (Fig. 5G–I). These data suggested that free DOX was pumped out of the cells by membrane P-gp transporter and thereby could hardly accumulate in MCF-7/ADR cells.[48–50] However, when MCF-7/ADR cells were incubated with PEG–DOX for 5 h, red fluorescence was clearly observed in the cytoplasm of tumor cells (Fig. 5J–L). These findings indicate that PEG–DOX nanoparticles may bypass the

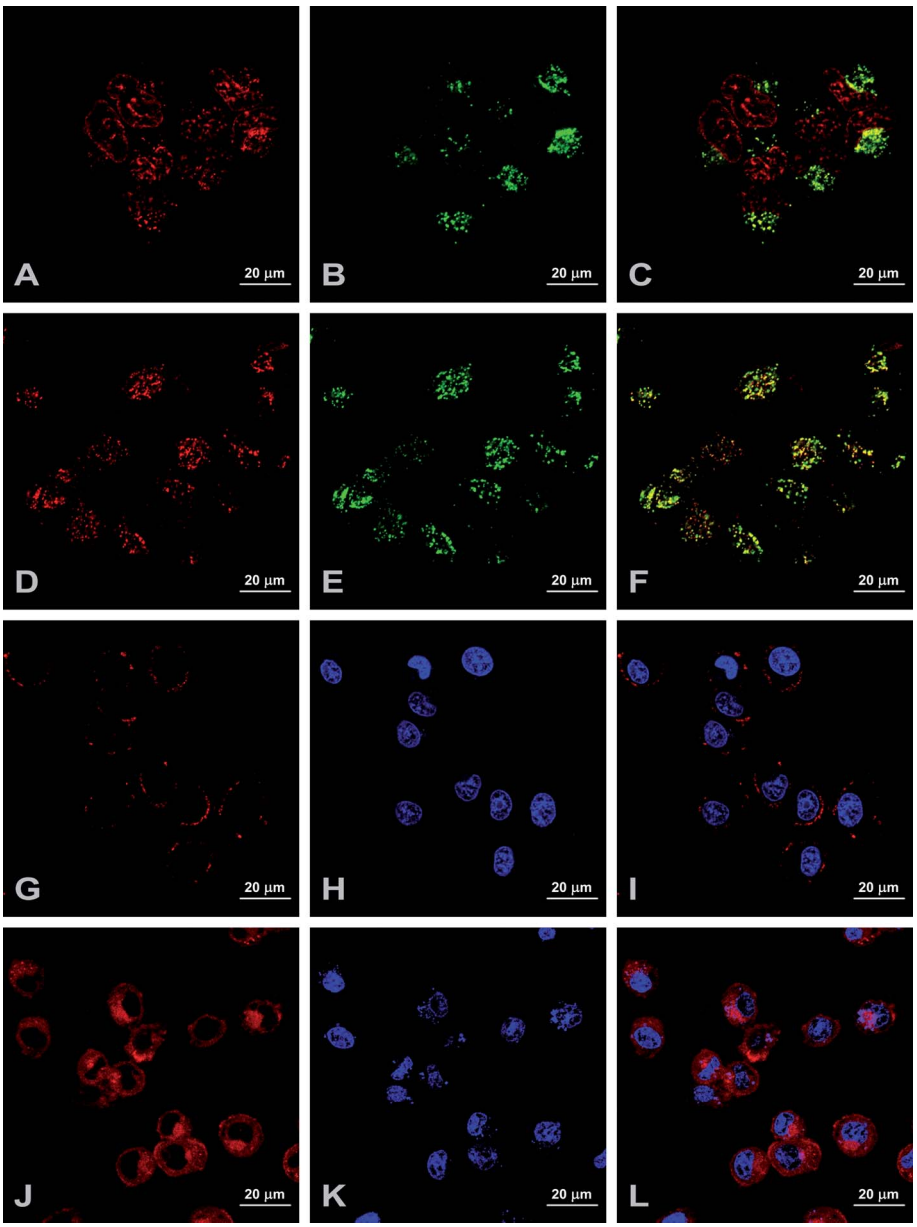

Fig. 5 Cellular uptake and intracellular localization of free DOX and PEG–DOX in tumor cells observed by confocal laser scanning microscopy. SKOV3 cells were incubated with free DOX (A–C) and PEG–DOX (D–F) at 37 °C for 5 h; MCF-7/ADR cells were incubated with free DOX (G–I) and PEG–DOX (J–L) at 37 °C for 5 h. (A and D) DOX channel (red); (B and E) Lyso-Tracker channel (green); (C and F) overlay of DOX and Lyso-Tracker channels; (G and J) DOX channel (red); (H and K) DRAQ-5 channel (blue); (I and L) overlay of DOX and DRAQ-5 channels.

drug resistance mediated by membrane transporters such as P-gp, and significantly enhance the internalization and accumulation of DOX in MDR tumors. Further *in vivo* investigations with mice bearing both sensitive and MDR tumors are currently ongoing in our laboratory.

3.5 *In vivo* antitumor activity and cardiotoxicity

In this preliminary animal study, a dose close to the MTD of DOX was used in order to simultaneously observe the *in vivo* anticancer efficacy and safety of PEG–DOX nanoparticles. As summarized in Fig. 6, although the tumor growth was almost completely inhibited after DOX treatment ($p < 0.001$, compared to the control group, Fig. 6A), the body weight of this group of animals sharply decreased ($p < 0.001$, compared to control and PEG–DOX groups, Fig. 6B), suggesting that severe toxic side effects were induced by DOX at the given dose. Eventually, we had to terminate all the animals in the DOX group on day 12 for humanitarian reasons. Indeed, the severe toxic side effects of free DOX were further demonstrated by the histopathological examination of the heart tissue, as alterations of tissue architecture and even apparent necrosis (inside the red circle) of cardiomyocytes were observed in mice treated with free DOX (Fig. 7). When animals were treated with PEG–DOX at an

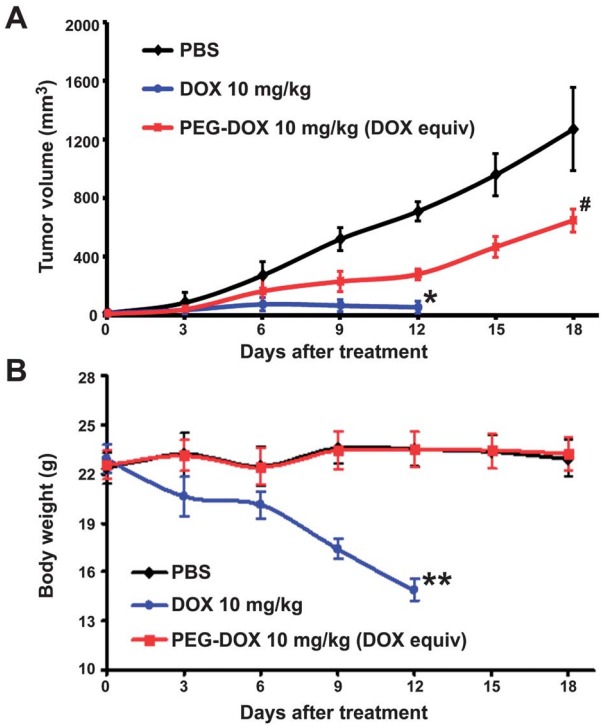

Fig. 6 Tumor volume (A) and body weight change (B) in nude mice bearing SKOV3 human ovarian xenograft tumors treated with PBS (◆), 10 mg kg^{-1} free DOX (●), PEG–DOX nanoparticles (10 mg kg^{-1} DOX equivalent dose, ■) *via* tail veins every three days. Data are presented as mean ± standard deviations (SD), $n = 4$. #, $P < 0.001$ when compared with the PBS group (day 0–12); *, $P < 0.001$ when compared with the PBS group and $P < 0.05$ when compared with the PEG–DOX group (day 0–12); **, $P < 0.001$ when compared with the PBS and PEG–DOX groups (day 0–12).

equivalent dose, the Inhibition Rate (IR) of tumor growth induced by PEG–DOX was 43% ($p < 0.001$, compared to the control group, Fig. 6A). Importantly, no obvious toxic side effects were observed even after six cycles of PEG–DOX treatment, and the body weight change of the PEG–DOX group was quite similar to the control group ($p > 0.05$, Fig. 6B). Further histological studies indicated that many tumor cells in tissues obtained from PEG–DOX or DOX groups exhibited excessive vacuolization, enlarged cell size, significantly decreased cellularity and typical apoptotic characteristics; that is, they were composed of membrane-bound, small nuclear fragments surrounded by a rim of cytoplasm (Fig. 7).[43,51–53] These data demonstrated that compared to free DOX, PEG–DOX nanoparticles have significantly increased *in vivo* safety and exert excellent therapeutic activity in animal models, which deserves further preclinical and even clinical studies.

4 Conclusions

In this study, we successfully designed and synthesized a self-assembling doxorubicin prodrug, PEG–DOX, by directly conjugating hydrophobic doxorubicin with a very short chain of PEG *via* a acid-cleavable hydrazone bond. We demonstrated that amphiphilic PEG–DOX can self-assemble into nanoparticles, and has extremely high (~46 wt%) and stable drug loading due to the low molecular weight of PEG. PEG–DOX nanoparticles are quite stable in PBS but release DOX much faster at pH 4.0 and 5.0. Interestingly, PEG–DOX could bypass P-gp-mediated efflux of free DOX *via* the endocytosis pathway, leading to significant drug accumulation in resistant MCF-7/ADR cells. Further studies demonstrated that PEG–DOX exhibits excellent *in vitro*

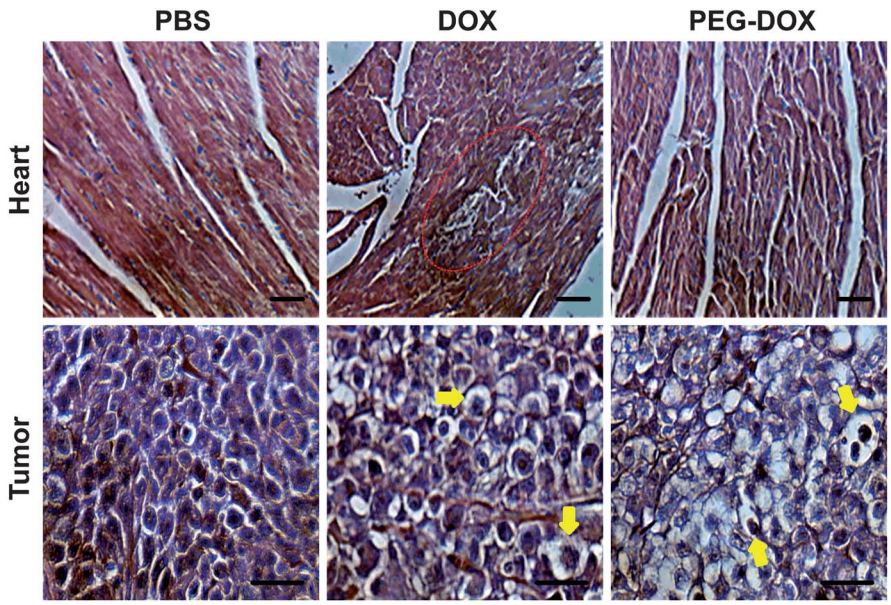

Fig. 7 H&E staining of the corresponding heart and tumor tissue sections obtained from nude mice bearing SKOV3 xenograft tumors, after treating with PBS, 10 mg kg^{-1} free DOX and PEG-DOX nanoparticles (10 mg kg^{-1} DOX equivalent dose), respectively, as described in the Experimental section. Area inside the red circle emphasizes alteration of tissue architecture and necrosis of cardiomyocytes. Note that the tumor group treated with free DOX and PEG-DOX showed larger cell size, decreased cellularity and more apoptotic cells containing small nuclear fragments surrounded by a narrow rim of cytoplasm (indicated by arrows) when compared with the group treated with PBS. Scale bar = 50 μm.

and *in vivo* antitumor activities, while it has no obvious toxic side effects even at a dosage equivalent to MTD of free DOX. PEG–DOX is a novel prodrug that may overcome various drawbacks of free DOX, and meanwhile has more advantages than many reported DOX-delivery systems in multiple aspects such as extremely high drug loading, controlled drug release and high *in vivo* safety. PEG–DOX may become an alternative to free DOX, and further studies on this promising prodrug are ongoing in our research group.

Acknowledgements

The authors thank the National Fund for Distinguished Young Scholars (50888001 to Y. Shen), and National Science Foundation of China (20974096 to Y. Shen, 21104065 to M. Sui), Program for Changjiang Scholars and Innovative Research Team in the University of China (to Y. Shen).

References

1 S. M. Swain, F. S. Whaley, M. C. Gerber, M. S. Ewer, J. R. Bianchine and R. A. Gams, *J. Clin. Oncol.*, 1997, **15**, 1333–1340.
2 R. P. Ahern and M. E. Gore, *J. Clin. Oncol.*, 1995, **13**, 726–732.
3 A. M. Murad, F. F. Santiago, A. Petroianu, P. R. S. Rocha, M. A. G. Rodrigues and M. Rausch, *Cancer*, 1993, **72**, 37–41.
4 S. E. Lipshultz, S. D. Colan, R. D. Gelber, A. R. Perezatayde, S. E. Sallan and S. P. Sanders, *N. Engl. J. Med.*, 1991, **324**, 808–815.
5 C. Carvalho, R. X. Santos, S. Cardoso, S. Correia, P. J. Oliveira, M. S. Santos and P. I. Moreira, *Curr. Med. Chem.*, 2009, **16**, 3267–3285.
6 K. M. Tewey, T. C. Rowe, L. Yang, B. D. Halligan and L. F. Liu, *Science*, 1984, **226**, 466–468.
7 G. Minotti, P. Menna, E. Salvatorelli, G. Cairo and L. Gianni, *Pharmacol. Rev.*, 2004, **56**, 185–229.
8 G. N. Hortobagyi, *Drugs*, 1997, **54**, 1–7.
9 A. U. Buzdar, C. Marcus, T. L. Smith and G. R. Blumenschein, *Cancer*, 1985, **55**, 2761–2765.
10 E. A. Lefrak, J. Pitha, S. Rosenhei and J. A. Gottlieb, *Cancer*, 1973, **32**, 302–314.
11 S. M. Swain, F. S. Whaley and M. S. Ewer, *Cancer*, 2003, **97**, 2869–2879.
12 L. Brannon-Peppas and J. O. Blanchette, *Adv. Drug Delivery Rev.*, 2004, **56**, 1649–1659.
13 N. Nasongkla, E. Bey, J. M. Ren, H. Ai, C. Khemtong, J. S. Guthi, S. F. Chin, A. D. Sherry, D. A. Boothman and J. M. Gao, *Nano Lett.*, 2006, **6**, 2427–2430.
14 E. R. Gillies and J. M. J. Frechet, *Drug Discovery Today*, 2005, **10**, 35–43.
15 A. Sharma and U. S. Sharma, *Int. J. Pharm.*, 1997, **154**, 123–140.
16 R. Duncan, *Nat. Rev. Cancer*, 2006, **6**, 688–701.
17 O. Lyass, B. Uziely, R. Ben-Yosef, D. Tzemach, N. I. Heshing, M. Lotem, G. Brufman and A. Gabizon, *Cancer*, 2000, **89**, 1037–1047.
18 P. A. Vasey, S. B. Kaye, R. Morrison, C. Twelves, P. Wilson, R. Duncan, A. H. Thomson, L. S. Murray, T. E. Hilditch, T. Murray, S. Burtles, D. Fraier, E. Frigerio, J. Cassidy and I. I. I. C. Canc Res Campaign Phase, *Clin. Cancer Res.*, 1999, **5**, 83–94.
19 Y. Matsumura, T. Hamaguchi, T. Ura, K. Muro, Y. Yamada, Y. Shimada, K. Shirao, T. Okusaka, H. Ueno, M. Ikeda and N. Watanabe, *Br. J. Cancer*, 2004, **91**, 1775–1781.
20 L. W. Seymour, D. R. Ferry, D. Anderson, S. Hesslewood, P. J. Julyan, R. Poyner, J. Doran, A. M. Young, S. Burtles, D. J. Kerr and I. I. I. C. Canc Res Campaign Phase, *J. Clin. Oncol.*, 2002, **20**, 1668–1676.
21 H. Maeda, J. Wu, T. Sawa, Y. Matsumura and K. Hori, *J. Controlled Release*, 2000, **65**, 271–284.
22 H. Maeda, in *Adv. Enzyme Regul., Vol. 41*, ed. G. Weber, Pergamon-Elsevier Science Ltd, Oxford, 2001, pp. 189–207.
23 H. S. Yoo and T. G. Park, *J. Controlled Release*, 2004, **96**, 273–283.
24 S. Y. Park and H. S. Yoo, *Int. J. Pharm.*, 2010, **383**, 178–185.
25 M. Prabaharan, J. J. Grailer, S. Pilla, D. A. Steeber and S. Q. Gong, *Biomaterials*, 2009, **30**, 5757–5766.
26 H. S. Yoo and T. G. Park, *J. Controlled Release*, 2001, **70**, 63–70.
27 L. Zhou, R. Cheng, H. Q. Tao, S. B. Ma, W. W. Guo, F. H. Meng, H. Y. Liu, Z. Liu and Z. Y. Zhong, *Biomacromolecules*, 2011, **12**, 1460–1467.
28 A. K. Singla, A. Garg and D. Aggarwal, *Int. J. Pharm.*, 2002, **235**, 179–192.
29 C. E. Soma, C. Dubernet, D. Bentolila, S. Benita and P. Couvreur, *Biomaterials*, 2000, **21**, 1–7.
30 F. M. Veronese, O. Schiavon, G. Pasut, R. Mendichi, L. Andersson, A. Tsirk, J. Ford, G. F. Wu, S. Kneller, J. Davies and R. Duncan, *Bioconjugate Chem.*, 2005, **16**, 775–784.
31 R. B. Greenwald, *J. Controlled Release*, 2001, **74**, 159–171.
32 R. B. Greenwald, Y. H. Choe, J. McGuire and C. D. Conover, *Adv. Drug Delivery Rev.*, 2003, **55**, 217–250.
33 C. Y. Long, M. M. Sheng, B. He, Y. Wu, G. Wang and Z. W. Gu, *Chin. J. Polym. Sci.*, 2012, **30**, 387–396.
34 F. M. Veronese and G. Pasut, *Drug Discovery Today*, 2005, **10**, 1451–1458.
35 D. Bhadra, S. Bhadra, S. Jain and N. K. Jain, *Int. J. Pharm.*, 2003, **257**, 111–124.
36 M. T. Peracchia, E. Fattal, D. Desmaele, M. Besnard, J. P. Noel, J. M. Gomis, M. Appel, J. d'Angelo and P. Couvreur, *J. Controlled Release*, 1999, **60**, 121–128.
37 M. Hruby, C. Konak and K. Ulbrich, *J. Controlled Release*, 2005, **103**, 137–148.
38 K. Ulbrich, T. Etrych, P. Chytil, M. Jelinkova and B. Rihova, *J. Controlled Release*, 2003, **87**, 33–47.
39 Y. Q. Shen, E. L. Jin, B. Zhang, C. J. Murphy, M. H. Sui, J. Zhao, J. Q. Wang, J. B. Tang, M. H. Fan, E. Van Kirk and W. J. Murdoch, *J. Am. Chem. Soc.*, 2010, **132**, 4259–4265.

40 J. Yang, W. W. Liu, M. H. Sui, J. B. Tang and Y. Q. Shen, *Biomaterials*, 2011, **32**, 9136–9143.
41 N. Toyota, F. R. Strebel, L. C. Stephens, H. Matsuda, T. Oshiro, G. N. Jenkins and J. M. C. Bull, *Int. J. Cancer*, 1998, **76**, 499–505.
42 D. Vetvicka, M. Hruby, O. Hovorka, T. Etrych, M. Vetrik, L. Kovar, M. Kovar, K. Ulbrich and B. Rihova, *Bioconjugate Chem.*, 2009, **20**, 2090–2097.
43 M. H. Sui, F. Chen, Z. Chen and W. M. Fan, *Int. J. Cancer*, 2006, **119**, 712–717.
44 O. J. Arola, A. Saraste, K. Pulkki, M. Kallajoki, M. Parvinen and L. M. Voipio-Pulkki, *Cancer Res.*, 2000, **60**, 1789–1792.
45 X. W. Liu, C. Chua, J. P. Gao, Z. Y. Chen, C. L. C. Landy, R. Hamdy and B. H. L. Chua, *Am. J. Physiol.: Heart Circ. Physiol.*, 2004, **286**, H933–H939.
46 G. Molineux, *Cancer Treat. Rev.*, 2002, **28**, 13–16.
47 N. Tang, G. J. Du, N. Wang, C. C. Liu, H. Y. Hang and W. Liang, *J. Natl. Cancer Inst.*, 2007, **99**, 1347.
48 C. F. Higgins, *Nature*, 2007, **446**, 749–757.
49 T. Litman, T. E. Druley, W. D. Stein and S. E. Bates, *Cell. Mol. Life Sci.*, 2001, **58**, 931–959.
50 M. M. Gottesman, T. Fojo and S. E. Bates, *Nat. Rev. Cancer*, 2002, **2**, 48–58.
51 J. F. R. Kerr, C. M. Winterford and B. V. Harmon, *Cancer*, 1994, **73**, 2013–2026.
52 L. Milas, N. R. Hunter, B. Kurdoglu, K. A. Mason, R. E. Meyn, L. C. Stephens and L. J. Peters, *Cancer Chemother. Pharmacol.*, 1995, **35**, 297–303.
53 R. Rajan, A. Poniecka, T. L. Smith, Y. Yang, D. Frye, L. Pusztai, D. J. Fiterman, E. Gal-Gombos, G. Whitman, R. Rouzier, M. Green, H. Kuerer, A. U. Buzdar, G. N. Hortobagyi and W. F. Symmans, *Cancer*, 2004, **100**, 1365–1373.

